Reversible Copper(II)/(I) Electrochemical Potential Switching Driven by Visible Light-Induced Coordinated Ring Rotation

Michihiro Nishikawa, Kuniharu Nomoto, Shoko Kume,* and Hiroshi Nishihara*

Department of Chemistry, School of Science, The University of Tokyo, 7-3-1 Hongo, Bunkyo-ku, Tokyo 113-0033, Japan

Ⓢ *Supporting Information*

ABSTRACT: We here describe the first metal complex system in which electronic signals can be repeatedly extracted by converting bistable states related to an intramolecular ligand rotational motion, which is fueled by visible light. The molecular structure for relating an electron transfer and a motion consists of a copper center and a coordinated unsymmetrically substituted pyrimidine derivative, whose rotational isomerization causes an electrochemical potential shift. To harness light energy effectively through metal-to-ligand charge transfer (MLCT) excitation, we prepared a simple copper(I) complex coordinated by a 4-methyl-2-(6′-methyl-2′-pyridyl)pyrimidine and a bulky diimine. The thermodynamic and kinetic parameters of redox and rotational reactions were analyzed by cyclic voltammograms at variable temperatures, by considering four stable isomers related to copper(II)/(I) states and rotational isomeric states. The key feature of this compound is that the rotation is frozen in the copper(I) state (rate constant for the rotation, $k_{Ii \to o} = 10^{-4}$ s^{-1}) but is active in the copper(II) state ($k_{IIi \to o} = 10^{-1}$ s^{-1}) at 203 K. The compound makes a bypass route to the isomeric metastable copper(I) state, via a tentative copper(II) state formed by photoelectron transfer (PET) in the presence of a redox mediator, decamethylferrocenium ion (DMFc$^+$), or upon a partial oxidation of the complex. Light- and heat-driven rotation in the copper(I) state with a potential shift ($\Delta E^{\circ\prime} = 0.14$ V) was analyzed by electrochemical measurements of the complex in the solution state. The rotor could be reset to the initial state by heating, thereby completing the cycle and enabling repeated operation fueled by light energy. A significant redox potential shift associated with the copper(II)/(I) transition accompanied the rotation, thereby providing a new type of molecular signaling system.

■ INTRODUCTION

Multistable molecules that are capable of intramolecular structural or chemical transitions form a subclass of molecules useful in nanotechnology applications, such as in single-electron transistors,[1,2] molecular electronics,[3−7] magnetic ordering,[8−10] artificial photosynthesis,[11,12] photochromic materials,[10,13−25] and molecular machines.[6,7,25−38] Redox-active molecules, in which oxidation states are reversibly switched by electronic stimuli, are one of the key components in these molecular devices. Redox-active molecules can be functionalized with photoswitchable ability by attaching photochromic molecules,[18−24] such as azobenzene[21,22] and diarylethene.[23,24]

The activities of multistable molecules as functional units within single molecules are frequently observed in natural systems.[39−41] For example, proton gradient energies across membranes can be converted to chemically high-energy ATP molecules via rotational motion of the F$_0$ unit of ATPase, where proton receptors are ultimately fabricated. Ferrocene-attached unidirectional motion driven by electronic voltages has been proposed as an energy-converting function acting like a natural motor.[42] The central goal in this field is to harness the natural motor functions of molecules that can convert the energy of external stimuli into useful responses based on the capacities of molecular motion.

To develop an electrochemical potential response from an artificial molecular rotor with a stimulus-convertible function, we have focused on simple copper coordination compounds with bidentate diimines, because of the well-established unique relationship between reversible redox activities, photophysics, and coordination structures in these compounds.[43−52] The copper(I) state prefers a tetrahedral geometry, whereas the copper(II) state favors a square planar geometry or a 5- or 6-coordinated form due to Jahn−Teller effects.[36−38,43−56] The structural changes associated with electron transfer events turn out to play a significant role in the function of copper blue proteins.[57−59] As a result, crowded coordination geometry generally renders the oxidation of copper(I) to copper(II) thermodynamically less favorable due to destabilization by steric repulsion in the copper(II) state.[43,44] For example, the oxidation potential of [Cu(dmp)$_2$]$^+$ (dmp = 2,9-dimethyl-1,10-phenanthroline) is much more positive than that of [Cu(phen)$_2$]$^+$ (phen = 1,10-phenanthroline).[43,44] In addition, copper(I) polypyridyl complexes basically exhibit an absorption band in the visible light region due to the metal-to-ligand charge transfer (MLCT) transition.[47−51] Introducing bulky substituents, such as a methyl group,[50,51] around the copper center strongly enhances its luminescence on account of the long-lived MLCT electronic excited state;[47−51] application of the luminessive copper(I) complexes into optical devices has

been developed by considering the steric effect around the copper center.[60−63] The MLCT state facilitates the photoelectron transfer (PET) process,[43,44,64] as in ruthenium(II) polypyridyl complexes.[65] Furthermore, bidentate diimines on copper undergo ligand substitution reactions at minute-scale rates at ambient temperatures.[53,54]

These unique properties enable us to design a molecule whose structural responses can be converted into a different signal form. We previously examined azobenzene-appended bipyridine ligands that undergo an electric potential shift via a reversible photoisomerization through an intermediate stabilized by ligand exchange at the copper center (i.e., the transition was not intramolecular).[66,67] To embed the ligand exchange within a single molecular process, we introduced a bidentate ligand that includes a coordinated pyrimidine moiety.[68−73] The ligand can effectively alternate between two possible pyrimidine nitrogen atom coordination geometries at the copper center via rotational isomerization. As the alpha substituents on the alternate pyrimidine nitrogen atoms are different, rotational isomerization alters the steric interactions within the coordination sphere at the copper center. The steric effects cause a shift of the redox potential by favoring either a tetrahedral geometry (preferred by copper(I)) or a square planar geometry (5- or 6-coordinated form preferred by copper(II)).[43,44] Rotational isomerization of the bidentate ligand therefore displays dual redox potentials, the electric signal of which can be detected in the cyclic voltammogram for the copper(II)/(I) couple.[68−71] Copper complexes that include unsymmetrically substituted pyrimidines, such as 4-methyl-2-(2′-pyridyl)pyrimidine, can undergo structural transitions based on the chemical energy supplied by adding redox reagent solutions.[68,69] The structural transitions modulate the electrode potential[68] and can manipulate intramolecular electron transfer within a redox array comprising a copper center and a bound ferrocene moiety.[69]

The major problem to be solved in this system is how best to drive the pyrimidine rotational isomerization in the energetically uphill direction to extract a responsive electric signal repeatedly. In the present work, we succeeded in driving this rotational isomeric system using visible light illumination through a PET process for the first time (Figure 1). The simplicity of the motion enabled us to accurately tailor the dynamics of the system. The structure of the copper complex was carefully designed to optimize sensitivity to photoillumination, by considering the sensitivity of the copper(I) complex excited state to steric factors.[47−51] We employed a 4-methyl-2-(6′-methyl-2′-pyridyl)pyrimidine (MepmMepy) li-
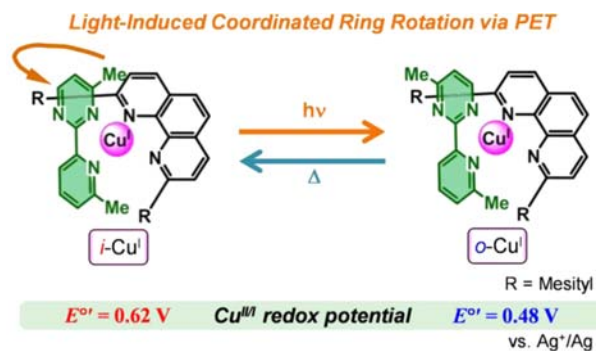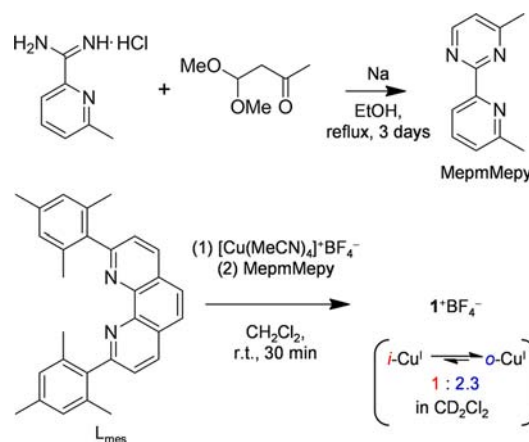
gand, which is similar to our previously described ligand but includes an additional methyl group at the 6-position of the pyridyl moiety. The additional methyl group is expected to extend the MLCT excited state lifetime.[47−51] 2,9-Dimesityl-1,10-phenanthroline (L_{mes}) was used as an auxiliary ligand because the bulky mesityl group yielded a similar MLCT lifetime extension; L_{mes} also helps prevent undesirable formation of a homoleptic complex.[74−77]

■ RESULTS AND DISCUSSION

Synthesis and Characterization. MepmMepy was newly synthesized by a condensation of a reported amidine[78,79] with acetylacetoaldehyde dimethylacetal, according to the modified procedure described in the literature.[80] A new compound, $[Cu(MepmMepy)(L_{mes})]^+BF_4^-$ ($1^+BF_4^-$), was synthesized by a reaction of tetrakis(acetonitrile)copper(I) tetrafluoroborate ($[Cu(MeCN)_4]^+BF_4^-$) with MepmMepy and L_{mes}[74,75] in dichloromethane at room temperature,[81] according to the slightly modified procedures described in our previous literature (Scheme 1).[68] The interconversion between coordi-

Scheme 1. Synthesis of $1^+BF_4^-$

nation isomers is described in Figure 1, where the notation of inner (*i-*) and outer (*o-*) isomers indicates the direction of the pyrimidine ring.

X-ray structural analysis of $1^+BF_4^-·CH_2Cl_2·0.5$hexane reveals that both *i-* and *o-*coordination forms were present in the same crystal (Figure 2a and Supporting Information Figure S1). The crystal structure was treated as a disorder between the *i-* and *o-*
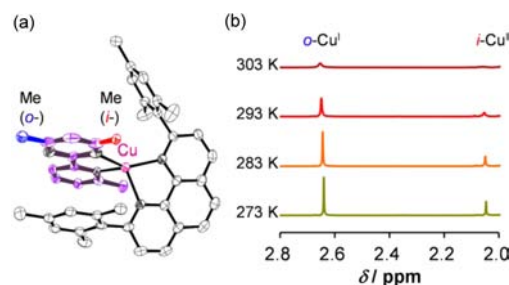

Figure 1. Conceptual diagram showing the photodriven and heat-driven pyrimidine ring rotational isomerization of $1^+BF_4^-$.

Figure 2. (a) ORTEP view of $1^+BF_4^-·CH_2Cl_2·0.5$hexane. The displacement ellipsoids are drawn at a 50% probability level. Hydrogen atoms, counteranions, crystal solvents, and one complex cation are omitted for clarity. (b) Temperature dependence of the methyl signal on the pyrimidine moiety in the ^1H NMR spectrum in CD_2Cl_2 in the dark.

forms, considering that the isomeric structures are almost identical, except for the position of the methyl group. Occupancy refinement of the disorder gave a i-Cu^I/o-Cu^I isomer ratio = 1:2.3.

The rotational behavior of $\mathbf{1}^+BF_4^-$ in a solution state was investigated by nuclear magnetic resonance (NMR) spectroscopy. The ^1H NMR spectrum in dichloromethane-d_2 at 273 K shows two sets of signals, which were assigned to i-Cu^I and o-Cu^I according to their chemical shifts, after consideration of the shielding effects of the copper and L_{mes} moieties (Figure 2b and Supporting Information Figure S2). Broadening of the peaks upon heating indicates that the two isomers coexisted and interconverted via rotational motions (Figures 2b and S3). The molar ratio of i-Cu^I and o-Cu^I, estimated from signal integration, remained fixed at 1:2.3 over the range 200−300 K (Figure S3).

Electrochemistry. Two requirements are required to manipulate an electron transfer via rotation processes: (i) the copper(II)/(I) redox potential between i- and o- isomers is different, and (ii) the rotational interconversion can be frozen and activated at an accessible temperature range.[68,69] We conducted cyclic voltammetry, as it provides information on both redox properties and rotation dynamics.

A voltammogram at 203 K in Bu_4NBF_4−CH_2Cl_2 at a scan rate of both 250 and 50 mV s^{-1} showed two reversible waves derived from two isomers at $E^{\circ\prime}$ = 0.48 and 0.62 V vs Ag^+/Ag (Figure 3a). The waves at 0.48 and 0.62 V were assigned to the
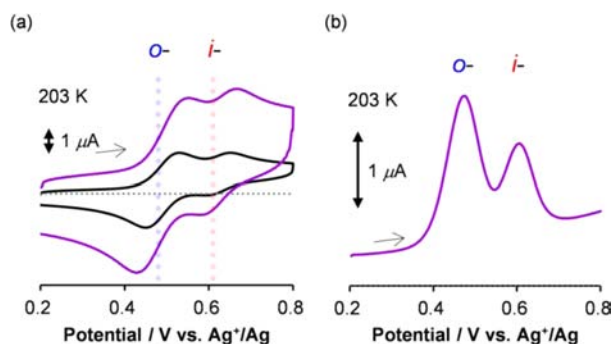

Figure 3. (a) Cyclic voltammograms of $\mathbf{1}^+BF_4^-$ (0.45 mM) in 0.1 M $Bu_4N^+BF_4^-$−CH_2Cl_2 at a scan rate of 250 (purple line) and 50 mV s^{-1} (black line) at 203 K. (b) Differential pulse voltammogram under the same conditions as for part a.

o-$Cu^{II/I}$ and i-$Cu^{II/I}$ redox reactions, respectively, as a bulky substituent around the copper center shifted the potential toward positive values by preventing the square planar geometry favored in the copper(II) state.[43,44] The prominence of the wave at $E^{\circ\prime}$ = 0.48 V compared with that at $E^{\circ\prime}$ = 0.62 V was consistent with the molar ratios of isomers estimated from ^1H NMR measurements. A differential pulse voltammogram showed both o-$Cu^{II/I}$ and i-$Cu^{II/I}$ waves, where the peak currents reflect the molar ratio of i-Cu^I and o-Cu^I in the solution (Figure 3b). Repeated potential sweeps in cyclic voltammetry gave identical current ratios of the isomers. The nice reversibility of these two waves suggests that four states, i-Cu^I, o-Cu^I, i-Cu^{II}, and o-Cu^{II}, are sufficiently stable without subsequent chemical degradation. A reduction wave of $\mathbf{1}^+BF_4^-$ was not observed with potential sweeps down to −1.8 V (Supporting Information Figure S4).

As the temperature was increased to 225 K at a scan rate of 250 mV s^{-1} (Figure 4a, purple line), the cathodic wave for i-
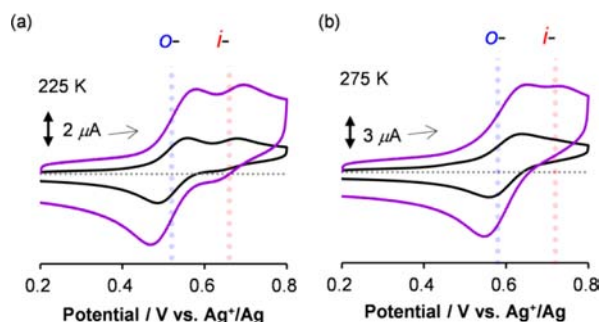

Figure 4. Cyclic voltammograms of $\mathbf{1}^+BF_4^-$ (0.45 mM) in 0.1 M $Bu_4N^+BF_4^-$−CH_2Cl_2 at a scan rate of 250 (purple line) and 50 mV s^{-1} (black line) at 225 K (a) and 275 K (b) in the dark.

Cu^{II} slightly decreased; the decrease was more apparent at a scan rate of 50 mV s^{-1} (Figure 4a, black line). Further warming to 275 K caused a transformation of the entire voltammogram, as if there was one cathodic wave (Figure 4b, purple line). The convergence into a single wave suggests that oxidation promotes a rotation from i- to o- on the time scale of the potential sweep.[56,83] The preference of the square planar geometry in the copper(II) state converted i-Cu^{II} into o-Cu^{II} because of steric repulsion of the methyl group via a thermally activated process. From the voltammograms, it appears as if there is a single reversible redox process when both interconversions in copper(II) and copper(I) states are sufficiently rapid, as compared with the potential scan at 50 mV s^{-1} (shown in Figure 4b).

Thermodynamics and Kinetics for the Rotation. As described above, we deduced that the shape of the voltammogram is mostly determined by the competence of the potential sweep and the nature of the rotational processes. A quantitative simulation analysis using cyclic voltammograms provides further constraints on the experimental conditions at which photodriven i-Cu^I → o-Cu^I rotation can be achieved.[56,83] We assumed a square scheme (Figure 5a) between four stable isomers, i-Cu^I, o-Cu^I, i-Cu^{II}, and o-Cu^{II}, and reproduced the experimental voltammograms at several temperatures. These simulations provide thermal and kinetic parameters for the redox potentials and rotations in both copper(I) and copper(II) states, as described in Table 1 and Supporting Information Figure S5 and Table S2.[56,83]

The equilibrium constant for the rotation in the copper(I) state (K_I), which was set as [o-isomer]/[i-isomer], remained 2.3 over the temperature range 200−300 K (Figure 5b). This result indicates that the two isomers were comparably stable. In contrast, a much larger equilibrium constant in the copper(II) state (K_{II}), obtained from the electrochemical analysis, indicates that nearly all molecules were present as the o-isomer under equilibrated conditions (Figure 5b).

The rate constant for the i- → o- rotation, estimated from the Arrhenius plots in the copper(I) state ($k_{Ii\to o}$), was less than 10^{-4} s^{-1} at 203 K, which indicates that the rotational motion was substantially frozen, which we call the "rotation-*OFF* state" (Figure 5c and d). When the temperature was raised to 250 K, $k_{Ii\to o}$ increased to 10^{-1} s^{-1}, indicating that the rotation was sufficiently activated from *OFF* to *ON* in the copper(I) state. At the intermediate temperature of 225 K, $k_{Ii\to o}$ was 10^{-3} s^{-1}, implying that the rotation proceeded slowly over a period of several minutes, which enabled us to trace the time progression of the rotational conversion. In contrast, the rate constant in the copper(II) state ($k_{IIi\to o}$) was 10^{-1} s^{-1}, even at 203 K,

10545

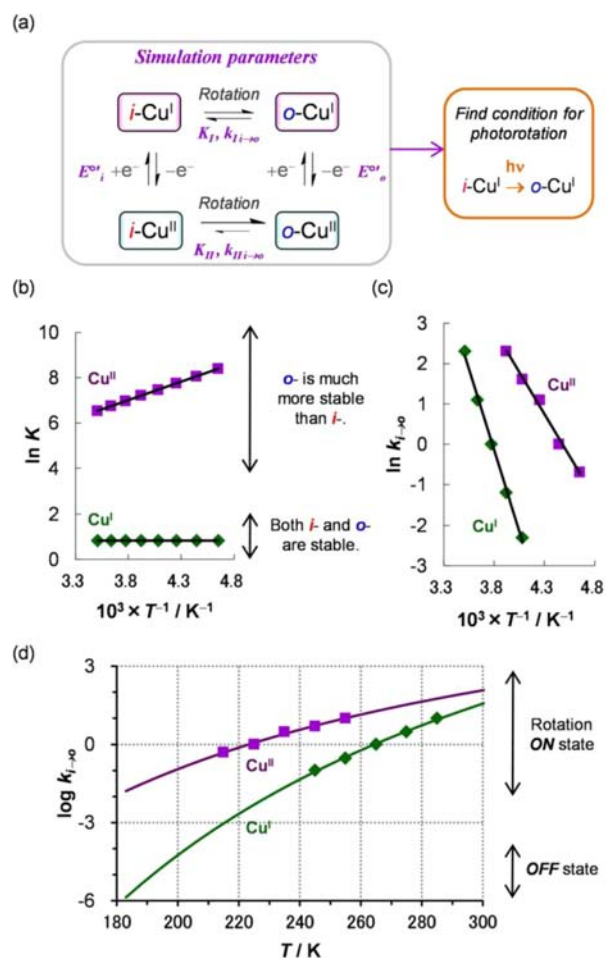dx.doi.org/10.1021/ja3028873 | J. Am. Chem. Soc. 2012, 134, 10543−10553

Figure 5. (a) Illustration for an aim of the simulation analysis based on the square scheme comprising the redox reaction (vertical) and the pyrimidine ring rotation (horizontal). (b, c) The van't Hoff plots (b) and the Arrhenius plots (c) for the $i\text{-} \rightarrow o\text{-}$ rotational equilibrium in the copper(I) (green dots) and copper(II) (purple dots) states in 0.1 M $Bu_4N^+BF_4^-$–CH_2Cl_2 in the dark. (d) The rate constants for the $i\text{-} \rightarrow o\text{-}$ ligand geometry isomerization in the copper(I) and copper(II) states as a function of temperature, estimated from the Arrhenius plots. Values determined from a simulated fit to the experimental cyclic voltammograms are shown as dots. Regression curves of the Arrhenius plots are indicated by lines.

Table 1. Selected Parameters Obtained from the Simulated Cyclic Voltammograms of $1^+BF_4^-$ at Scan Rates of 250, 100, 50, and 25 mV s^{-1} in 0.1 M $Bu_4N^+BF_4^-$ –CH_2Cl_2

	285 K	265 K	245 K	225 K	200 K
$E^{\circ\prime}{}_o$/V^a	0.59	0.57	0.55	0.52	0.48
$E^{\circ\prime}{}_i$/V^b	0.73	0.71	0.69	0.66	0.62
$K_I{}^c$	2.3	2.3	2.3	2.3	2.3
$K_{II}{}^d$	7×10^2	1×10^3	2×10^3	3×10^3	8×10^3
$k_{Ii \rightarrow o}$/s^{-1} ^{e}	10	1	0.1	<0.1	<0.1
$k_{IIi \rightarrow o}$/s^{-1} ^{f}	>10	>10	5	1	<0.1

^{a}Redox potential for $o\text{-}Cu^{II/I}$, vs Ag$^+$/Ag. ^{b}Redox potential for $i\text{-}Cu^{II/I}$, vs Ag$^+$/Ag. ^{c}Equilibrium constant, set as $[o\text{-}Cu^I]/[i\text{-}Cu^I]$. ^{d}Equilibrium constant, set as $[o\text{-}Cu^{II}]/[i\text{-}Cu^{II}]$. ^{e}Rate constant for the $i\text{-}Cu^I \rightarrow o\text{-}Cu^I$ rotation. ^{f}Rate constant for the $i\text{-}Cu^{II} \rightarrow o\text{-}Cu^{II}$ rotation.

indicating that the rotation was active on the time scale of one minute (rotation-*ON* state) (Figure 5c and 5d).[84]

These results suggest that we can thermally capture a metastable copper(I) state out of the *i-/o-* equilibrium at 203 K, if light converts a coordination isomer into another form. Also, the metastable state can be reset to its initial state by heating to 250 K, at which thermal rotation proceeds to the equilibrium state within several seconds. The unique heat-induced *ON–OFF* switching of the rotation process in the copper(I) state is a key phenomenon for photoinduction of our rotational system.

Photophysical Properties. To fuel the rotational isomerization of $1^+BF_4^-$ by light illumination, we examined the absorption and luminescence spectra of $1^+BF_4^-$. The absorption spectrum of $1^+BF_4^-$ in CH_2Cl_2 is shown in Figure 6a. A characteristic absorption band in the visible region ($\lambda_{max} =$
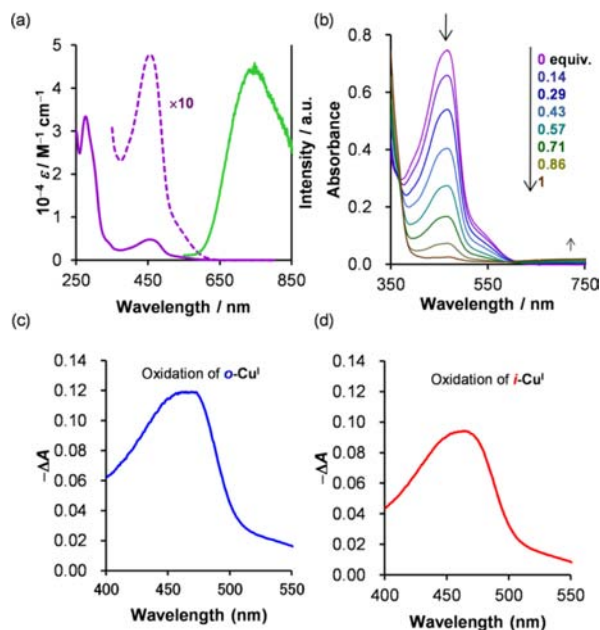

Figure 6. (a) UV–vis spectra of $1^+BF_4^-$ in CH_2Cl_2 at room temperature: absorption spectrum in the dark (purple); absorption spectrum in the dark, ×10 (dashed purple); emission spectrum (green). (b) Absorption spectra of $1^+BF_4^-$ in the dark upon addition of 0, 0.14, 0.29, 0.43, 0.57, 0.71, 0.86, and 1.0 equiv of $(NH_4)^+{}_2[Ce\text{-}(NO_3)_6]^{2-}$ in acetone at 193 K. (c, d) Differences in absorption spectra of $1^+BF_4^-$ in acetone at 193 K in the dark upon oxidation with $(NH_4)_2[Ce(NO_3)_6]$ between 0.14 equiv and 0.29 equiv (c), and between 0.71 equiv and 0.86 equiv (d).

456 nm, $\varepsilon = 4.8 \times 10^3$ M^{-1} cm^{-1}) was attributed to a transition from the ground state to the singlet MLCT excited state, which appears generally in the bis(diimine)copper(I) complex family.[47−49] The absorption spectra of $1^+BF_4^-$ in acetone at both 293 and 193 K were similar to those in dichloromethane. The rotational behavior in acetone was also very similar to that in dichloromethane (Supporting Information Figures S6 and S7 and Table S3).

The difference between the absorption spectra of $o\text{-}Cu^I$ and $i\text{-}Cu^I$ was examined, on the basis of spectral changes upon oxidation of $1^+BF_4^-$, as follows. The absorption spectral changes of $1^+BF_4^-$ upon addition of 0, 0.14, 0.29, 0.43, 0.57, 0.71, 0.86, and 1.0 equiv $(NH_4)^+{}_2[Ce(NO_3)_6]^{2-}$ (ammonium hexanitratocerate (IV))[85] in acetone at 193 K are shown in Figure 6b. The oxidation diminished the MLCT absorption band of copper(I) complexes and increased a weak $d–d$ transition band of copper(II) complexes.[43−56] The oxidation reaction of $i\text{-}Cu^I$ and $o\text{-}Cu^I$ (with the ratio, 1:2.3) proceeded
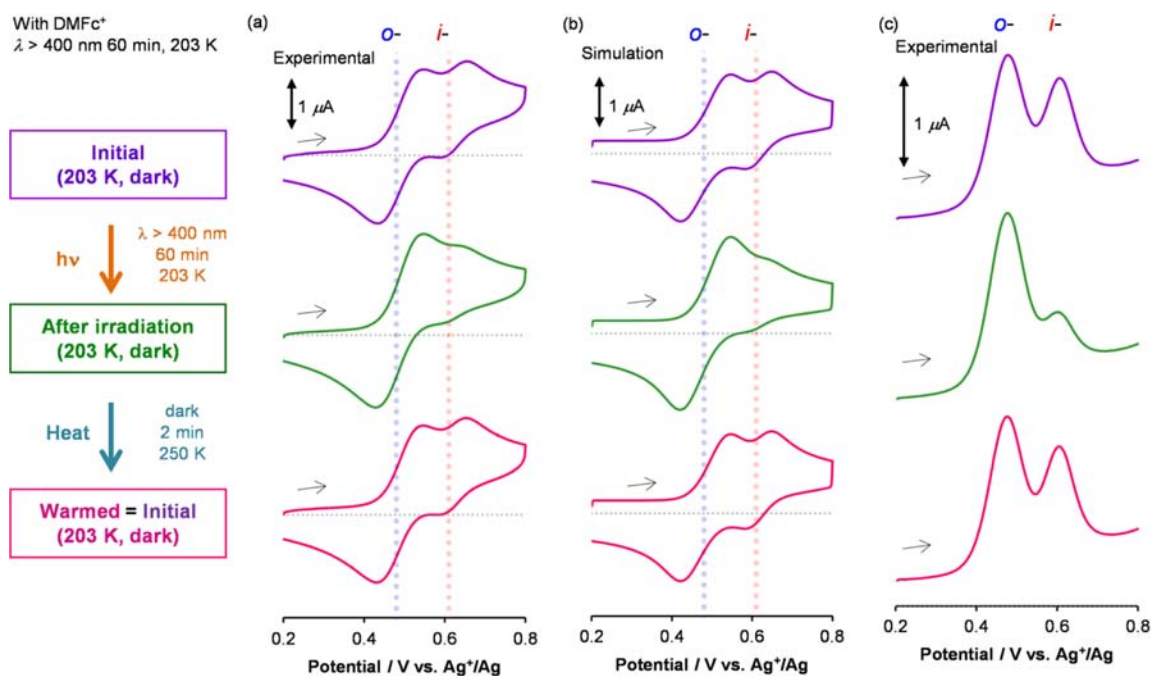
Figure 7. Photorotation experiments in the DMFc$^+$ system with notes about the procedures. Experimental (a) and simulated (b) cyclic voltammograms at a scan rate of 50 mV s^{-1}, and experimental differential pulse voltammograms (c). Investigated DMFc$^+$ systems comprise **1**$^+$BF$_4^-$ (0.45 mM) in 0.1 M Bu$_4$N$^+$BF$_4^-$–CH$_2$Cl$_2$ containing 1.8 mM DMFc$^+$BF$_4^-$ at 203 K in the dark. Top: initial state (purple lines). Middle: after 60 min of visible light irradiation ($\lambda > 400$ nm) at 203 K (green lines). Bottom: after 2 min of heating at 250 K in the dark (pink lines).

almost independently, because the rotation was frozen at 193 K. As o-Cu^I is oxidized more easily than i-Cu^I, the early (from 0 to 0.7 equiv) and later (from 0.7 to 1.0 equiv) spectral changes qualitatively show absorption changes of o-Cu^I and i-Cu^I upon oxidation, respectively. The changes in the region from 400 to 500 nm reflect the absorption of o-Cu^I and i-Cu^I, as MLCT absorption is much more intense than that of the d−d transition of copper(II) complexes.

Figure 6c and d display the differences in absorption spectra upon oxidation in the early (0.14 → 0.29 equiv, where only o-Cu^I is oxidized) and later (0.71 → 0.86 equiv, where only i-Cu^I is oxidized) spectral changes, respectively. As the absorption change is constant during the addition of (NH$_4$)$^+{}_2$[Ce-(NO$_3$)$_6$]$^{2-}$, the difference in absorption between o-Cu^I and i-Cu^I would be small. The small absorption difference is similar to that in our previous rotational system, based on a copper complex coordinated by 4-methyl-2-(2′-pyridyl)pyrimidine and 2,9-bis(9-anthryl)-1,10-phenanthroline as ligands.[68] It should be noted that introducing methyl substituents into ligands of a bis(diimine)copper(I) family slightly affects their absorption spectra, within several nanometers of the maximum absorption change.[50,51] The absorption spectra of the solutions were reversed by chemical reduction using decamethylferrocene (DMFc^0), suggesting that oxidation of **1**$^+$BF$_4^-$ proceeds without the subsequent chemical degradation (Supporting Information Figure S8).

The redox potential of the excited state of **1**$^+$BF$_4^-$, which is important for constructing a strategy for PET-driven i-Cu^I → o-Cu^I rotational processes, can be estimated using its luminescence spectra.[86] A broad emission band from **1**$^+$BF$_4^-$ in CH$_2$Cl$_2$ was observed in the red region ($\lambda_{max} = 750$ nm) (Figure 6a). It should be noted that this emission band may have arisen predominantly from the i-isomer, as the steric hindrance among substituents around the copper(I) center significantly increases the emission efficiency.[47−51]

The energy difference between the ground and excited states was estimated at ca. 1.6 eV from the maxima of the emission spectra.[86] The copper(II)/(I) redox potential of the ground state of the i-isomer was 0.62 V vs Ag$^+$/Ag; thus, the redox potential of the excited i-Cu^I state was ca. −1.0 V, sufficient for oxidation by the decamethylferrocenium ion (DMFc$^+$) with a reduction potential of −0.4 V. The transiently formed copper(II) complex would be expected to return to the copper(I) state by the subsequent back electron transfer process. The copper(II)/(I) redox potential values for both the i- and o-isomers were sufficiently positive to reoxidize DMFc^0. This estimation was also supported by the facts that similar copper(I) polypyridyl complexes undergo PET fairly efficiently,[43,44] and DMFc$^{+/0}$ works as an excellent redox mediator.[87]

Photorotation of 1$^+$ with Redox Mediator. The above results provide a basis for controlling a photoinduced rotation. The PET process is likely to form a tentative copper(II) state, which can make a bypass from i-Cu^I to o-Cu^I, as the activation energy for rotation in copper(II) is less than that in copper(I). In addition, DMFc can be a potential electron acceptor to complete the PET scheme.

The voltammograms of **1**$^+$BF$_4^-$ in Bu$_4$NBF$_4$−CH$_2$Cl$_2$ at several temperatures in the dark were not altered by addition of 4 equiv of DMFc$^+$BF$_4^-$ ($E^{\circ\prime} = -0.41$ V vs Ag$^+$/Ag at 200 K, and −0.35 V vs Ag$^+$/Ag at 275 K), suggesting that DMFc$^+$ does not disturb thermal rotational dynamics (Figures 3 and 7 and Supporting Information Figures S5 and S9). Since DMFc$^+$ does not oxidize **1**$^+$BF$_4^-$ (redox potentials: o-Cu$^{II/I}$ = 0.89 V vs DMFc$^{+/0}$, i-Cu$^{II/I}$ = 1.03 V vs DMFc$^{+/0}$), the ratio of rotational isomers, i-Cu^I/o-Cu^I/i-Cu^{II}/o-Cu^{II}, is 1:2.3:0:0. For clarity, we hereafter describe only the rotational isomer ratio i-Cu^I/o-Cu^I.

In the presence of 4 equiv of DMFc$^+$ (1.8 mM), the cyclic voltammogram of a solution containing **1**$^+$BF$_4^-$ (0.45 mM) was significantly altered upon photoirradiation in Bu$_4$N$^+$BF$_4^-$−

CH$_2$Cl$_2$. The experimental procedures and results of this DMFc$^+$ system are summarized in Figure 7. Prior to photoirradiation (Figure 7a top, purple lines), two redox waves, one each for the *i*- and *o*-isomers in a ratio of 1:2.3, were observed. The shape of the voltammograms remained constant in the dark, demonstrating that there were no ongoing processes in the absence of photoirradiation (Supporting Information Figure S10). At 60 min, with photoirradiation with visible light ($\lambda > 400$ nm) at 203 K, the redox waves gradually converged to a wave corresponding to the *o*-isomer (Figure 7a middle, green lines). The shapes of the voltammograms after photoirradiation did not change with incubation at 203 K in the dark for 10 min, reflecting the persistence of the irradiated state (Figure S10). Subsequent heating for 2 min at 250 K in the dark recovered the initial voltammogram, indicating thermal relaxation of the light-induced metastable state (Figure 7a bottom, pink lines). The ratios of *i*-Cu^I to *o*-Cu^I in the initial, photoirradiated, and recovered states estimated from a simulated model fit to the cyclic voltammograms (Figure 7b) were 1:2.3, 1:8, and 1:2.3, respectively.[83] Changes in the differential pulse voltammograms of the solution during the process corresponded to the changes in the cyclic voltammograms (Figure 7c).

Figure 8 displays the changes in the peak current for the *o*-Cu$^{II/I}$ anodic wave in the experimental cyclic voltammograms
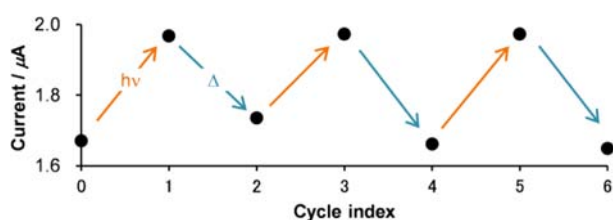

Figure 8. Changes in the anodic peak current at 0.55 V in the experimental cyclic voltammograms of **1**$^+$BF$_4^-$ (0.45 mM) in 0.1 M Bu$_4$N$^+$BF$_4^-$−CH$_2$Cl$_2$ containing 1.8 mM DMFc$^+$BF$_4^-$ at 203 K.

(Supporting Information Figure S11) upon repeated operations with alternating light irradiation and heating. The process worked repeatedly, demonstrating that the photoinduced isomerization and the redox switching were reversible (Figure 8). These results clearly demonstrate a reversible change in the molar ratios of isomers based on photodriven and heat-driven rotational isomerization

The convergence of redox waves at 203 K in the DMFc$^+$ system with visible light irradiation was negligible after 5 min, considerable after 20 min, and nearly saturated after 60 min (Table 2 and Supporting Information Figure S12). As selective irradiation with blue light ($\lambda = 450 \pm 40$ nm) also induced isomerization from the *i*- to the *o*-isomer, isomerization could have resulted from excitation of the MLCT absorption band (Table 2). Because photoisomerization did not occur in the absence of DMFc$^+$, a reaction pathway through PET from copper(I) complexes to the electron acceptor (DMFc$^+$) appeared to be a key step for the *i*- to *o*-conversion (Table 2). It should be noted that 20 min of visible light irradiation at 225 K did not alter the voltammogram (Table 2); these results are discussed in the final section.

Figure 9a shows the schematic representation of photorotation in the DMFc$^+$ system. The observed photodriven and heat-driven isomerization mechanisms can be interpreted in terms of the kinetics of the transition between the preferred

Table 2. Photorotation Experiments under Several Conditions Using Cyclic Voltammograms

entry	$t/$min[a]	$\lambda/$nm[b]	DMFc$^+/$equiv[c]	$T/$K[d]	changes in *i*-Cu$^I/o$-Cu^I[e]
1	5	>400	4	203	negligible
2	20	>400	4	203	1:2.3 → 1:6
3	60	>400	4	203	1:2.3 → 1:8
4	60	450 ± 40	4	203	1:2.3 → 1:4
5	60	>400	0	203	negligible
6	20	>400	4	225	negligible

[a]Irradiation time. [b]Irradiation wavelength. [c]Chemical equivalent of DMFc$^+$BF$_4^-$ to total **1**$^+$BF$_4^-$. [d]Temperature. [e]Changes in *i*-Cu$^I/o$-Cu^I upon light irradiation, judging from a simulated model fit to the experimental cyclic voltammograms of **1**$^+$BF$_4^-$ (0.45 mM) containing 1.8 mM DMFc$^+$BF$_4^-$ in 0.1 M Bu$_4$NBF$_4$−CH$_2$Cl$_2$ at a scan rate of 50 mV s^{-1} in the dark at T K before and after light irradiation. All voltammograms are displayed in Figure S12 of the Supporting Information.
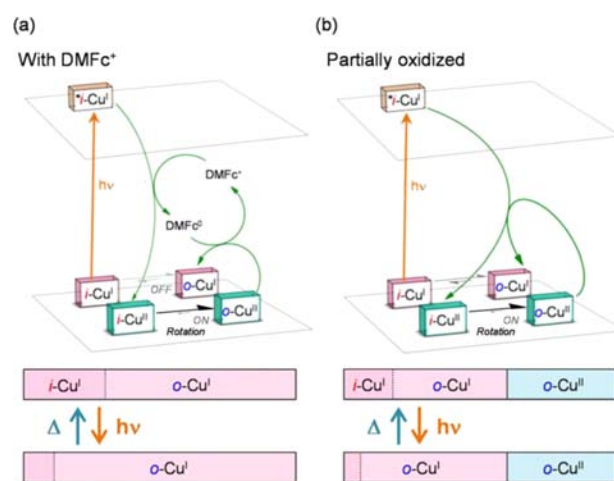

Figure 9. (a, b) Schematic representation of the PET-driven *i*-Cu^I to *o*-Cu^I ligand geometry isomerization of (a) **1**$^+$BF$_4^-$ in the presence of DMFc$^+$ and (b) the partial oxidation of **1**$^+$BF$_4^-$ by (NH$_4$)$^+{}_2$[Ce-(NO$_3$)$_6$]$^{2-}$. The reversible changes in the molar ratios of the isomers upon light irradiation and heating are illustrated in the bottom panels.

ligand geometries of the copper(I) and copper(II) states, obtained from simulation fits to the voltammograms (Figure 5). The *i*- and *o*-isomers are present in the initial copper(I) state in a ratio of 1:2.3 ($K_I = [o\text{-Cu}^I]/[i\text{-Cu}^I] = 2.3$). Photoirradiation of the solution induces PET from the excited *i*-Cu^I state (**i-Cu^I) to the electron acceptor (DMFc$^+$), as the oxidation potential of **i-Cu^I is −1.0 V. The transiently formed *i*-Cu^{II} isomerizes to *o*-Cu^{II} for two reasons: (i) the ligand geometric transition within the copper(II) state was not frozen ($k_{IIi\rightarrow o} = 10^{-1}$ s^{-1}, in the ON state); and (ii) *i*-Cu^{II} was thermodynamically unfavorable as compared with *o*-Cu^{II}, on account of large steric repulsion ($K_{II} = [o\text{-Cu}^{II}]/[i\text{-Cu}^{II}] > 10^2$). Finally, the transiently formed *o*-Cu^{II} is reduced to *o*-Cu^I through a back-electron transfer reaction with DMFc^0. The net process proceeds through the conversion of *i*-Cu^I to *o*-Cu^I. If the forward conversion rate constant is sufficiently larger than the thermally activated reverse rate constant (from *o*-Cu^I to *i*-Cu^I, $k_{Io\rightarrow i} = 10^{-4}$ s^{-1} at 203 K, in the OFF state), the photodriven *i*-Cu$^I \rightarrow o$-Cu^I ligand isomerization proceeds. Therefore, the rate of *i*-Cu$^I \rightarrow o$-Cu^I photorotation is greater than 10^{-4} s^{-1} in the DMFc$^+$ system at 203 K. The photorotation induces the change in a ratio of *i*-Cu$^I/o$-Cu^I (in

10548

dx.doi.org/10.1021/ja3028873 | *J. Am. Chem. Soc.* 2012, 134, 10543−10553

the conditions of Figure 7, from 1:2.3 to 1:8). The reversion from the light-induced metastable state by the thermal process at 203 K would take on the order of 10^4 s, judging from the rate constant value, $k_{Io \to i} = 10^{-4}$ s^{-1}. Heating to 250 K ($k_{Io \to i} = 10^{-1}$ s^{-1}, in the *ON* state) provides sufficient thermal energy to the copper complex that the initial ratio of isomers is restored through back-isomerization. Consequently, the results show that the i-Cu$^I \to o$-Cu^I rotation via the redox potential shift in the DMFc$^+$ system can be driven by light.[88]

Photorotation from i-Cu^I to o-Cu^I under Partial Oxidation. We next attempted to construct a combined photorotation-redox switching system without the need for an electron mediator, to show its high versatility. The mechanism described above predicts that a more efficient reversible transition is expected if the copper(II) complex itself acts as an electron acceptor ($E°' = 0.48$ V), in place of the relatively weaker DMFc$^+$ state ($E°' = -0.41$ V) (Figure 9b).

To test this speculation, $\mathbf{1}^+$BF$_4^-$ in Bu$_4$N$^+$BF$_4^-$−CH$_2$Cl$_2$ was partially oxidized by 0.4 equiv of (NH$_4$)$^+_2$[Ce(NO$_3$)$_6$]$^{2-}$. The changes in the partially oxidized system with light irradiation and heating were basically similar to those of the DMFc$^+$ system, judging from the anodic waves in the voltammograms.

In this case, the sample contains four copper components, as it includes copper(II) species even in the dark condition. The ratio of each component was estimated as follows.

$$a = [o\text{-Cu}^{II}] + [i\text{-Cu}^{II}] \tag{1}$$

$$1 - a = [o\text{-Cu}^I] + [i\text{-Cu}^I] \tag{2}$$

$$x(1 - a) = [o\text{-Cu}^I] \tag{3}$$

$$[o\text{-Cu}^I] + [i\text{-Cu}^I] + [o\text{-Cu}^{II}] + [i\text{-Cu}^{II}] = 1 \tag{4}$$

in the dark, upon repeated operation with 60 min of visible light irradiation ($\lambda > 400$ nm) at 203 K and 2 min of heating at 250 K in the dark. The voltammograms are shown in Figure S11 of the Supporting Information.

Here, the total amount of copper(II) species is expressed as a, which is identical to an equivalent amount of oxidant. The ratio of o-Cu^I to total copper(I) species is expressed as x. Since the rotation in the copper(II) state is always under equilibrium, the molar ratio of i-Cu^{II} is negligible, considering its large equilibrium constant ($K_{II} = [o\text{-Cu}^{II}]/[i\text{-Cu}^{II}] > 10^2$). Therefore,

$$a = [o\text{-Cu}^{II}] + [i\text{-Cu}^{II}] \cong [o\text{-Cu}^{II}] \tag{5}$$

As $K_I = [o\text{-Cu}^I]/[i\text{-Cu}^I] = 2.3$ does not depend on temperature, x in the initial state is

$$x = K_I/(1 + K_I) = 0.7 \tag{6}$$

In the case of $a = 0.4$, the molar ratio in the initial state of the partial oxidation system is i-Cu^I/o-Cu^I/i-Cu^{II}/o-Cu^{II} = 1:2.3:0:2.2. Considering that the copper(II) state is always under equilibrium and that i-Cu^{II} can be set to 0, we describe the rotational isomer ratio only as i-Cu^I/o-Cu^I for clarity. Thus, oxidation of 0.75 mM $\mathbf{1}^+$BF$_4^-$ by 0.4 equiv of (NH$_4$)$^+_2$[Ce-(NO$_3$)$_6$]$^{2-}$ (0.30 mM) in Bu$_4$N$^+$BF$_4^-$−CH$_2$Cl$_2$ yields 0.45 mM of $\mathbf{1}^+$BF$_4^-$ solution with copper(II) complexes (0.30 mM) as redox mediator.

Cyclic voltammograms of the partially oxidized system noted above showed two anodic waves at 225 K, one each for the i- and o-isomers, in a ratio of 1:2.3, which reflects the ratio of i-Cu^I and o-Cu^I in the solution (Figure 10a top, purple line). No deformation of voltammograms in the dark occurred,

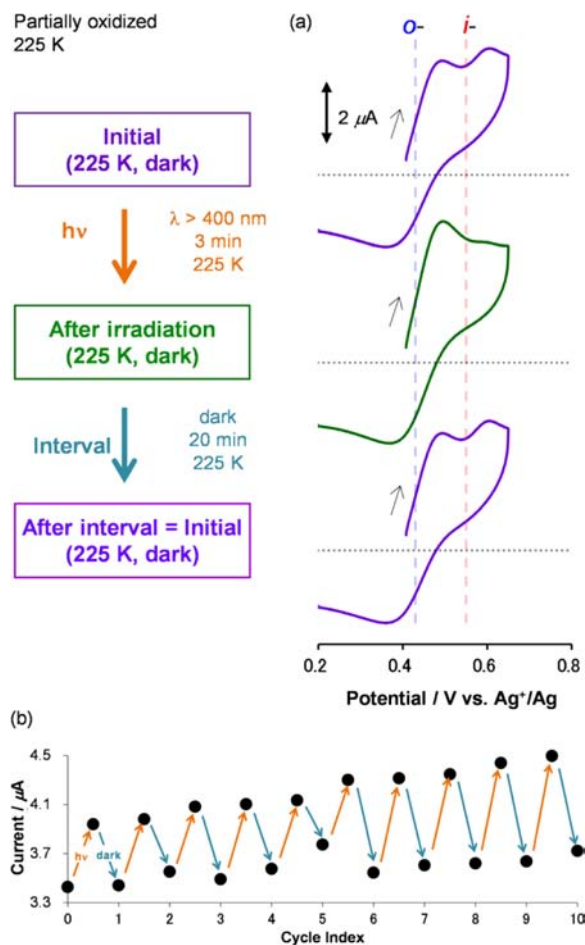**Figure 10.** (a) Experimental cyclic voltammograms at a scan rate of 100 mV s^{-1} of $\mathbf{1}^+$BF$_4^-$ (0.75 mM) in Bu$_4$N$^+$BF$_4^-$−CH$_2$Cl$_2$/acetone (v/v 20:1) upon addition of 0.4 equiv of (NH$_4$)$^+_2$[Ce(NO$_3$)$_6$]$^{2-}$ (0.3 mM) at 225 K in the dark. Top (purple line): initial state. Middle (green line): after 3 min of visible light irradiation ($\lambda > 400$ nm) at 225 K. Bottom (purple line): after a 20-min interval at 225 K in the dark. (b) Changes in the anodic peak current at 0.50 V at 225 K in the experimental cyclic voltammograms of the solution upon repeated operation with 3 min of visible light irradiation ($\lambda > 400$ nm) at 225 K and 20-min intervals at 225 K in the dark. The voltammograms are shown in Figure S14 of the Supporting Information.

suggesting that the expected self-exchange electron transfer between the copper species induced negligible changes in the ratios of rotational isomers (Figure S13 of the Supporting Information). The redox waves almost completely converged into a single wave corresponding to the o-isomer upon 3 min of photoirradiation with visible light ($\lambda > 400$ nm) at 225 K (Figure 10a middle, green line). The convergence can be qualitatively explained by a change in molar ratio from i-Cu^I/o-Cu^I = 1:2.3 to ca. 1:8, since the light-induced changes in the cyclic voltammograms resemble those of the DMFc$^+$ system from the viewpoint of anodic waves; simulation of the anodic waves also supported the molar ratio changes (Figure S13 and Table S4). The voltammograms gradually recovered to the initial state in the dark (Figure S14) and were completely restored after a 20-min interval (Figure 10a bottom, purple). Figure 10b displays the changes in anodic peak currents of the o-isomer in the cyclic voltammograms at 225 K in the partially oxidized system for 10 repeated operations (experimental voltammograms are displayed in Figure S15). The result shows

the excellent repeatability of the photorotation and redox switching.

The PET process of the partially oxidized system can be described as follows (Figure 9b). Photoirradiation of i-Cu^I followed by PET to o-Cu^{II} yields i-Cu^{II} and o-Cu^I, leading to a rapid rotational isomerization transition of i-Cu^{II} to o-Cu^{II}. The net scheme is i-Cu^I to o-Cu^I without back electron transfer to o-Cu^{II}, unlike in the DMFc$^+$-mediated system. It should be noted that the photorotation proceeds even at 225 K, unlike in the DMFc$^+$ system, and in a very short time frame. The rate of i-Cu$^I \rightarrow o$-Cu^I photorotation is greater than 10^{-3} s^{-1} in the partially oxidized system at 225 K, coincident with the competitive thermal back-isomerization process, with rate constant $k_{I_{o \rightarrow i}} = 10^{-3}$ s^{-1}. The scheme contributes considerably to changes in the molar ratio, i-Cu$^I/o$-Cu^I, from initial to metastable irradiated states (in Figure 10, from 1:2.3 to ca. 1:8). The rate constant of thermal reversion at 225 K is $k_{I_{o \rightarrow i}} = 10^{-3}$ s^{-1}, which qualitatively implies that the light-induced metastable state is restored to equilibrium after 10^3 s. The estimation is consistent with the 20-min recovery process displayed in the voltammogram at 225 K. Consequently, partial oxidation turns out to be an effective way to achieve the conversion of light stimuli to redox potentials through i-Cu$^I \rightarrow o$-Cu^I photorotation.

Factors Dominating Photorotation Rate. Upon studying the photorotation condition, we noticed that photorotation under partial oxidation proceeds much faster than in the presence of DMFc$^+$. The rate difference is beyond that attributable to concentration or temperature and, therefore, must originate from the rotation mechanism.

When we used DMFc$^+$ with 20 min of visible light irradiation at 225 K and at 200 K (Table 2), the light-induced voltammogram changes at 225 K were negligible, because the rate of o-Cu$^I \rightarrow i$-Cu^I thermal reversion at 225 K ($k_{I_{o \rightarrow i}} = 10^{-3}$ s^{-1}) overcomes that of photodriven i-Cu$^I \rightarrow o$-Cu^I. Photorotation in the DMFc$^+$ system, on the other hand, requires cooling to 200 K ($k_{I_{o \rightarrow i}} = 10^{-4}$ s^{-1}). As the conditions were identical, with the exception of temperature, we determined that the rate increment of $k_{I_{o \rightarrow i}}$ due to heating is larger than that of photorotation. In other words, the slow thermal reversion rate is a determining factor for photorotation at 200 K in the DMFc$^+$ system.

On the other hand, photorotation was observed at 225 K in a partially oxidized system (Figure 10). Possible variables in the experimental conditions of the two systems related to photorotation behavior are as follows: (i) temperature (225 K), (ii) concentrations of total copper(I) species (0.45 mM), (iii) light irradiation time (3 or 20 min), (iv) concentration of the redox mediator (0.30 mM or 1.8 mM), and (v) type of redox mediator (copper(II) complex or DMFc$^+$). Conditions (i) and (ii) are identical in both systems. Conditions (iii) and (iv) are considered to work against rapid rotation in a partially oxidized system, by decreasing the density of photons and the probability of collisions during intermolecular electron transfer. Therefore, enhancement of the photorotation rate must be related to redox mediator processes. In a comparison of the two photorotation schemes (Figure 9), the partial oxidation system does not require back electron transfer processes to complete the scheme. Also, the highly reducing driving force of o-Cu^{II} can contribute to the higher efficiency of photorotation in the partially oxidized system, as compared with the case in the DMFc$^+$ system. The expected slow rate of electron transfer in

copper(II)/(I) species may contribute to the efficiency of rotation processes.

Consequently, we succeeded in establishing two kinds of systems in which light stimuli are reversibly converted into copper(II)/(I) redox potentials via molecular rotation, but which exhibited different photorotation behaviors.

CONCLUSION

We demonstrated the conversion of light stimuli into electrochemical potential via reversibly working artificial molecular rotation. The energy-processing function was acquired by adding a photoresponse to a copper-coordinated pyrimidine ring rotation system, in which the molecular motion can be extracted as an electrochemical potential of the copper(II)/(I) redox reaction. A key feature of the present system is that the population of bistable isomers in the copper(I) state with different redox potentials ($\Delta E^{\circ\prime} = 0.14$ V) is reversibly converted by light and heat stimuli through a PET-induced process. The bistability is acquired by the high activation energy of the copper(I) state, which is drastically decreased in the transiently formed copper(II) state. PET processes can take a bypass route in the rotation of the copper(I) complex. The system works not only with a redox mediator but also upon partial oxidation, in which the copper complex itself considerably assists the photorotation, in contrast to the role of DMFc$^+$ in the DMFc$^+$ system.

Generally, photodriven bistable material changes are accompanied by significant color changes, which involve light absorption efficiency and reconstruction of the electronic state.[13−25] Our present photo- and heat-driven rotation system works without a significant color change or copper(I) ^{1}MLCT absorption, but it can induce electron transfer. It provides a further methodology to construct photodriven materials.

Since molecular electronics components such as transistor[1,2] and memory[7] work by charge injection, the present redox potential response can be progressed into other types of signals via intramolecular electron transfer. The function of the light-driven redox-synchronized molecular rotor can provide electronic, magnetic, and other molecular signaling characteristics.

EXPERIMENTAL SECTION

Materials. 6-Methyl-2-pyridinecarboximidamide monohydrochloride,[78,79] tetrakis(acetonitrile)copper(I) tetrafluoroborate,[89] 2,9-dimesityl-1,10-phenanthroline (L$_{mes}$),[74,75] and decamethylferrocenium tetrafluoroborate[90] were also prepared according to methods described in the literature. Other chemicals were used as purchased.

X-ray Structural Analysis. A red single crystal of 1^+BF$_4^-$·CH$_2$Cl$_2$·0.5hexane was obtained by diffusing hexane into a dichloromethane solution of 1^+BF$_4^-$. Diffraction data were collected with an AFC10 diffractometer coupled with a Rigaku Saturn charge-coupled device (CCD) system equipped with a rotating-anode X-ray generator producing graphite-monochromated Mo Kα radiation ($\lambda = 0.7107$ Å). Lorentz polarization and numerical absorption corrections were performed with the program Crystal Clear 1.3.6. The structure was solved by the direct method using SIR 92 software[91] and refined against F^2 using SHELXL-97.[92] WinGX software was used to prepare the material for publication.[93] The crystallographic data are listed in Table S1 of the Supporting Information. The isomeric structures were almost identical, except for the position of the methyl group. Occupancy refinement of the cyrstallographic disorder gave a i-/o- = 3:7 isomer ratio, as analyzed by the PART option of the SHELX-97 program. The disorders of the BF$_4^-$ molecules in the crystals were analyzed by the PART, ISOR, DELU, and SIMU options of the SHELX-97 program.

Instrumentation. Nuclear magnetic resonance spectra at several temperatures in the dark were recorded using a Bruker DRX 500 spectrometer, using a ca. 20 min data-recording interval. The ^{13}C NMR spectrum of MepmMepy was recorded using a JEOL ECX 400 spectrometer. The reported chemical shifts of the solvent residual peaks were used for calibration of the NMR spectra in chloroform-d_1 (CDCl$_3$, δ = 7.26 ppm for ^{1}H, δ = 77.16 ppm for ^{13}C) and dichloromethane-d_2 (CD$_2$Cl$_2$, δ = 5.32 ppm for ^{1}H).[82] UV−vis absorption spectra in the dark were recorded with a JASCO V-570 spectrometer and a Hewlett-Packard 8453 spectrometer equipped with a USP-203-A UNISOKU cryostat, using a quartz cell with a 1-cm optical path length. Steady-state corrected emission spectra were recorded with a HITACHI F-4500 spectrometer. Electrochemical measurements were recorded with an ALS 750A electrochemical analyzer (BAS. Co., Ltd.) and a HZ-3000 electrochemical analyzer (Hokuto Denko Co. Ltd.), each equipped with a UNISOKU cryostat. The working electrode was a 0.3 mm i.d. glassy carbon electrode; a platinum wire served as the auxiliary electrode, and the reference electrode was an Ag$^+$/Ag electrode (a silver wire immersed in 0.1 M Bu$_4$N$^+$ClO$_4^-$/0.01 M Ag$^+$ClO$_4^-$/CH$_3$CN). The solutions were deoxygenated with pure argon prior to the electrochemical measurements. Light irradiation was performed using a MAX-302 xenon lamp (ASAHI SPECTRA) equipped with an optical fiber with a long-pass filter (cut-on 400 nm) or a bandpass filter (central wavelength 450 nm, full width at half-maximum 80 nm).

Thermodynamic and Kinetic Analysis. The molar ratios of isomers of **1$^+$BF$_4^-$** in solution at several temperatures were determined from the ^{1}H NMR signal integration in the methyl group on the basis of pyrimidine moieties. The broad spectra at around room temperature were excluded from the thermodynamic analysis. The experimental cyclic voltammograms were simulated using BASi Digisim 3.03a software, based on two independent double-step electron transfer systems. The isomer equilibrium constants in the copper(II) state were derived from the experimentally obtained equilibrium constants of isomers in the copper(I) state and the two redox potentials of i- and o-isomers. The van't Hoff plots were based on an equilibrium constant of [o-isomer]/[i-isomer]. The molar ratios of isomers at variable temperatures were calculated from extrapolations of the van't Hoff plots. The rate constants for rotational processes from the i- to o-isomer were determined from the simulation analysis of the cyclic voltammograms. The rates of the rotations at various temperatures were calculated from the slopes and intercepts of the Arrhenius plots. The good fit of simulated curves with the experimental voltammograms confirmed the validity of the analyses.

Synthesis of 4-Methyl-2-(6′-methyl-2′-pyridyl)pyrimidine (MepmMepy). Under a nitrogen atmosphere, 6-methyl-2-pyridine-carboximidamide (1.0 g, 5.8 mmol) was dissolved in an ethanol solution of sodium ethoxide (prepared from 175 mg of sodium and 60 mL of ethanol) at room temperature. Acetylacetoaldehyde dimethyl-lacetal (1 mL, 8 mmol) was added to the mixture. The reaction mixture was refluxed for 3 days. The reaction mixture was cooled to room temperature and acidified with acetic acid. The solvent was evaporated and the residue dissolved in water and extracted with CH$_2$Cl$_2$. The organic layer was dried over sodium sulfate, filtered, and evaporated. The residue was chromatographed on an alumina gel column eluted with ethyl acetate−hexane (1:1 v/v). The solvent was evaporated to obtain a colorless powder: yield, 0.285 g (1.54 mmol, 27%). ^{1}H NMR (500 MHz, CDCl$_3$): δ 8.76 (d, J = 5.1 Hz, 1H), 8.29 (d, J = 7.8 Hz, 1H), 7.74 (t, J = 7.7 Hz, 1H), 7.26 (d, 1H), 7.16 (d, J = 5.1 Hz, 1H), 2.72 (s, 3H), 2.65 (s, 3H). ^{13}C NMR (100 MHz, CDCl$_3$): δ 24.7, 25.1, 119.9, 121.0, 124.7, 137.2, 154.7, 157.5, 159.1, 163.8, 168.0. Elemental analysis. Calculated for C$_{11}$H$_{11}$N$_3$: C 71.33, H 5.99, N 22.69. Found C 71.53, H 6.19, N 22.40.

Synthesis of [Cu(MepmMepy)(L$_{mes}$)]$^+$BF$_4^-$ (1$^+$BF$_4^-$). Under a nitrogen atmosphere, [Cu(MeCN)$_4$]$^+$BF$_4^-$ (28.3 mg, 0.0900 mmol) was added to L$_{mes}$ (37.1 mg, 0.0891 mmol) in 5 mL of CH$_2$Cl$_2$. To the resultant orange solution, MepmMepy (15.7 mg, 0.0848 mmol) was added, and the color of the solution changed immediately to dark red. The reaction mixture was stirred for 30 min. The solution was filtered, and diethyl ether (15 mL) was added to the solution to precipitate the

product, a deep red solid of **1$^+$BF$_4^-$**: yield, 42 mg (0.055 mmol, 65%). ^{1}H NMR (500 MHz, CD$_2$Cl$_2$ 273 K): δ 8.71−8.66 (m, i-3H + o-2H), 8.30 (d, J = 7.7 Hz, i-1H), 8.24 (d, J = 7.7 Hz, o-1H), 8.20 (s, i-2H), 8.19 (s, o-2H), 8.14 (d, J = 5.4 Hz, o-1H), 7.87−7.80 (m, i-3H + o-3H), 7.30 (d, J = 4.1 Hz, i-1H), 7.29 (d, J = 7.7 Hz, o-1H), 7.25 (d, J = 5.6 Hz, o-1H), 7.22 (d, J = 4.8 Hz, i-1H), 6.39 (s, i-2H), 6.33 (s, i-2H), 6.32 (s, o-2H), 6.28 (s, o-2H), 2.64 (s, o-3H), 2.05 (s, i-3H), 1.97 (s, o-3H), 1.95 (s, o-6H), 1.93 (s, i-6H), 1.90 (s, i-3H), 1.77 (s, o-6H), 1.69 (s, i-6H), 1.68 (s, o-6H), 1.61 (s, i-6H). Elemental analysis. Calculated for C$_{41}$H$_{39}$N$_5$CuBF$_4$·C$_{0.1}$H$_{0.2}$Cl$_{0.2}$: C 64.90, H 5.19, N 9.21. Found: C 64.71, H 5.33, N 8.92.

Monitoring of Photorotation from i-Cu^I to o-Cu^I in the Redox Mediator System. The electrochemical cell, shielded from room light by covering with aluminum foil, was equipped with electrodes, a cryostat, and the optical fiber connected to the xenon lamp. The electrochemical cells were interfaced with a cryostat container, whose size and shape fitted the cells. The opening between the cell and the container is filled with methanol. The electrochemical measurements were performed on the static solution at 203 K in the dark after vigorous stirring. Under an argon atmosphere, a 2 mL 0.1 M Bu$_4$N$^+$BF$_4^-$−CH$_2$Cl$_2$ solution of **1$^+$BF$_4^-$** (0.45 mM) was cooled at 203 K in the dark, followed by electrochemical measurements. Then, the solution was stirred and photoirradiated with visible light (λ > 400 nm) at 203 K for 60 min, followed by further measurements, which showed a negligible change in the voltammograms. Then, a 100 μL deoxygenated CH$_2$Cl$_2$ solution of DMFc$^+$BF$_4^-$ (1.8 mM, 4 equiv to **1$^+$BF$_4^-$**) was added to the solution at room temperature. The solution was cooled at 203 K in the dark, followed by measurements in the initial state. Then, the solution was stirred at 203 K in the dark for several minutes, followed by measurements to check that no changes were detected in the voltammogram with time. Then, the solution was stirred and photoirradiated with visible light (λ > 400 nm) at 203 K for 60 min, followed by measurements which showed considerable voltammogram changes. The solution was stirred at 203 K in the dark for several minutes, followed by measurements for the persistence of the irradiated state. After a 2-min heating of the solution to 250 K in the dark with stirring, the solution was cooled to 203 K in the dark, followed by measurements in the warmed state. The operations were repeated three times, with a 60-min photoirradiation at 203 K and a 2-min heating in the dark at 250 K, to achieve repeatable voltammogram changes. Then, the operations were performed using blue light (λ = 450 ± 40 nm) instead of visible light. The solution was heated to 225 K in the dark, followed by measurements performed at 225 K instead of at 203 K. The solution was stirred and photoirradiated with 20 min of visible light (λ > 400 nm) at 225 K, followed by measurements at 225 K, which showed a negligible change.

Monitoring of Photorotation from i-Cu^I to o-Cu^I in the Partially Oxidized System. The measurements were performed using the same electrochemical cell mentioned above. Electrochemical measurements were performed for the static solution at 225 K in the dark after vigorous stirring. Under an argon atmosphere, a 100 μL of a deoxygenated acetone solution of ammonium hexanitratocerate (IV) (0.3 mM, 0.4 equiv to **1$^+$BF$_4^-$**) was added to 2 mL of 0.1 M Bu$_4$N$^+$BF$_4^-$−CH$_2$Cl$_2$ solution of **1·BF$_4$** (0.75 mM) at room temperature. Then, the solution was cooled to 225 K in the dark, followed by measurements at the initial state. The solution was stirred and photoirradiated with visible light (λ > 400 nm) at 225 K for 3 min, followed by measurements in the irradiated state, which gave a considerable voltammogram change. The solution was stirred for 20 min at 225 K in the dark, followed by the measurements. The operation was repeated 10 times, with 3 min of visible light (λ > 400 nm) irradiation at 225 K followed by a 20-min interval at 225 K in the dark, to achieve a repeatable voltammogram change.

■ ASSOCIATED CONTENT

Ⓢ Supporting Information

Crystal structure data (CIF), spectral data, and electrochemical data. This material is available free of charge via the Internet at http://pubs.acs.org.

■ AUTHOR INFORMATION

Corresponding Author

kume@chem.s.u-tokyo.ac.jp; nisihara@chem.s.u-tokyo.ac.jp

Notes

The authors declare no competing financial interest.

■ REFERENCES

(1) Kubatkin, S.; Danilov, A.; Hjort, M.; Cornil, J.; Brédas, J.-L.; Stuhr-Hansen, N.; Hedegård, P.; Bjørnholm, T. *Nature* **2003**, *425*, 698−701.

(2) Park, J.; Pasupathy, A. N.; Goldsmith, J. I.; Chang, C.; Yaish, Y.; Petta, J. R.; Rinkoski, M.; Sthena, J. P.; Abruña, H. D.; McEuen, P. L.; Ralph, D. C. *Nature* **2002**, *417*, 722−725.

(3) Moth-Poulsen, K.; Bjørnholm, T. *Nat. Nanotechnol.* **2009**, *4*, 551−556.

(4) Joachim, C.; Gimzewski, J. K.; Aviram, A. *Nature* **2000**, *408*, 541−548.

(5) de Silva, A. P. *Nature* **2008**, *454*, 417−418.

(6) Flood, A. H.; Stoddart, J. F.; Steuerman, D. W.; Heath, J. R. *Science* **2004**, *306*, 2055−2056.

(7) Green, J. E.; Wook Choi, J.; Boukai, A.; Bunimovich, Y.; Johnston-Halperin, E.; DeIonno, E.; Luo, Y.; Sheriff, B. A.; Xu, K.; Shik Shin, Y.; Tseng, H.-R.; Stoddart, J. F.; Heath, J. R. *Nature* **2007**, *445*, 414−417.

(8) Simão, C.; Mas-Torrent, M.; Crivillers, N.; Lloveras, V.; Artés, J. M.; Gorostiza, P.; Veciana, J.; Rovira, C. *Nat. Chem.* **2011**, *3*, 359−364.

(9) Sato, O.; Iyoda, T.; Fujishima, A.; Hashimoto, K. *Science* **1996**, *272*, 704−705.

(10) Venkataramani, S.; Jana, U.; Dommaschk, M.; Sönnichsen, F. D.; Tuczek, F.; Herges, R. *Science* **2011**, *331*, 445−448.

(11) Imahori, H.; Guldi, D. M.; Tamaki, K.; Yoshida, Yu.; Luo, C.; Sakata, Y.; Fukuzumi, S. *J. Am. Chem. Soc.* **2001**, *123*, 6617−6628.

(12) Meyer, T. J. *Acc. Chem. Res.* **1989**, *22*, 163−170.

(13) Irie, M.; Fukaminato, T.; Sasaki, T.; Tamai, N.; Kawai, T. *Nature* **2002**, *420*, 759−760.

(14) Kobatake, S.; Takami, S.; Muto, H.; Ishikawa, T.; Irie, M. *Nature* **2007**, *446*, 778−781.

(15) Gorostiza, P.; Isacoff, E. Y. *Science* **2008**, *322*, 395−399.

(16) Beharry, A. A.; Sadovski, O.; Woolley, G. A. *J. Am. Chem. Soc.* **2011**, *133*, 19684−19687.

(17) Uchida, K.; Yamanoi, Y.; Yonezawa, T.; Nishihara, H. *J. Am. Chem. Soc.* **2011**, *133*, 9239−9241.

(18) Kume, S.; Nishihara, H. *Dalton Trans.* **2008**, 3260−3271.

(19) Muratsugu, S.; Kume, S.; Nishihara, H. *J. Am. Chem. Soc.* **2008**, *130*, 7204−7205.

(20) Sakamoto, R.; Murata, M.; Nishihara, H. *Angew. Chem., Int. Ed.* **2006**, *45*, 4793−4795.

(21) Nishihara, H. *Coord. Chem. Rev.* **2005**, *249*, 1468−1475.

(22) Kurihara, M.; Hirooka, A.; Kume, S.; Sugimoto, M.; Nishihara, H. *J. Am. Chem. Soc.* **2002**, *124*, 8800−8801.

(23) Fraysse, S.; Coudret, C.; Launay, J.-P. *Eur. J. Inorg. Chem.* **2000**, 1581−1590.

(24) Tanaka, Y.; Inagaki, A.; Akita, M. *Chem. Commun.* **2007**, 1169−1171.

(25) Muraoka, T.; Kinbara, K.; Aida, T. *Nature* **2006**, *440*, 512−515.

(26) Ruangsupapichat, N.; Pollard, M. M.; Harutyunyan, S. R.; Feringa, B. L. *Nat. Chem.* **2011**, *3*, 53−60.

(27) Fletcher, S. P.; Dumur, F.; Pollard, M. M.; Feringa, B. L. *Science* **2005**, *310*, 80−82.

(28) Hernández, J. V.; Kay, E. R.; Leigh, D. A. *Science* **2004**, *306*, 1532−1537.

(29) Serreli, V.; Lee, C.-F.; Kay, E. R.; Leigh, D. A. *Nature* **2007**, *445*, 523−527.

(30) Balzani, V.; Credi, A.; Venturi, M. *Molecular Devices and Machines*, 2nd ed.; Wiley-VCH: Weinheim, 2008.

(31) Kay, E. R.; Leigh, D. A.; Zerbetto, F. *Angew. Chem., Int. Ed.* **2007**, *46*, 72−191.

(32) Browne, W. R.; Feringa, B. L. *Nat. Nanotechnol.* **2006**, *1*, 25−35.

(33) Brouwer, A. M.; Frochot, C.; Gatti, F. G.; Leigh, D. A.; Mottier, L.; Paolucci, F.; Roffia, S.; Wurpel, G. W. H. *Science* **2001**, *291*, 2124−2128.

(34) Mobian, P.; Kern, J.-M.; Sauvage, J.-P. *Angew. Chem., Int. Ed.* **2004**, *43*, 2392−2395.

(35) Murakami, H.; Kawabuchi, A.; Kotoo, K.; Kunitake, M.; Nakashima, N. *J. Am. Chem. Soc.* **1997**, *119*, 7605−7606.

(36) Armaroli, N.; Balzani, V.; Collin, J.-P.; Gavina, P.; Sauvage, J.-P.; Ventura, B. *J. Am. Chem. Soc.* **1999**, *121*, 4397−4408.

(37) Collin, J.-P.; Dietrich-Buchecker, C.; Gaviña, P.; Jiménez-Molero, M. C.; Sauvage, J.-P. *Acc. Chem. Res.* **2001**, *34*, 477−487.

(38) Zahn, S.; Canary, J. W. *J. Am. Chem. Soc.* **2002**, *124*, 9204−9211.

(39) Dau, H.; Zaharieva, I. *Acc. Chem. Res.* **2009**, *42*, 1861−1870.

(40) Vale, R. D.; Milligan, R. A. *Science* **2000**, *288*, 88−95.

(41) Junge, W.; Sielaff, H.; Engelbrecht, S. *Nature* **2009**, *459*, 364−370.

(42) Vives, G.; Carella, A.; Launay, J.-P.; Rapenne, G. *Coord. Chem. Rev.* **2008**, *252*, 1451−1459.

(43) Ruthkosky, M.; Kelly, C. A.; Castellano, F. N.; Meyer, G. J. *Coord. Chem. Rev.* **1998**, *171*, 309−322.

(44) Ruthkosky, M.; Castellano, F. N.; Meyer, G. J. *Inorg. Chem.* **1996**, *35*, 6406−6412.

(45) Miller, M. T.; Gantzel, P. K.; Karpishin, T. B. *Inorg. Chem.* **1998**, *37*, 2285−2290.

(46) Itoh, S.; Funahashi, S.; Koshino, N.; Takagi, H. D. *Inorg. Chim. Acta* **2001**, *324*, 252−265.

(47) Armaroli, N.; Accorsi, G.; Cardinali, F.; Listorti, A. *Top. Curr. Chem.* **2007**, *280*, 69−115.

(48) Lavie-Cambot, A.; Cantuel, M.; Leydet, Y.; Jonusauskas, G.; Bassani, D. M.; McClenaghan, N. D. *Coord. Chem. Rev.* **2008**, *252*, 2572−2584.

(49) McMillin, D. R.; McNett, K. M. *Chem. Rev.* **1998**, *98*, 1201−1219.

(50) Everly, R. M.; Ziessel, R.; Suffert, J.; McMillin, D. R. *Inorg. Chem.* **1991**, *30*, 559−561.

(51) Cunningham, C. T.; Cunningham, K. L. H.; Michalec, J. F.; McMillin, D. R. *Inorg. Chem.* **1999**, *38*, 4388−4392.

(52) Iwamura, M.; Watanabe, H.; Ishii, K.; Takeuchi, S.; Tahara, T. *J. Am. Chem. Soc.* **2011**, *133*, 7728−7736.

(53) Desvergnes-Breuil, V.; Hebbe, V.; Dietrich-Buchecker, C.; Sauvage, J.-P.; Lacour, J. *Inorg. Chem.* **2003**, *42*, 255−257.

(54) Meyer, M.; Albrecht-Gary, A. M.; Dietrich-Buchecker, C. O.; Sauvage, J.-P. *Inorg. Chem.* **1999**, *38*, 2279−2287.

(55) Rorabacher, D. B. *Chem. Rev.* **2004**, *104*, 651−697.

(56) Le Poul, N.; Campion, M.; Douziech, B.; Rondelez, Y.; Le Clainche, L.; Reinaud, O.; Le Mest, Y. *J. Am. Chem. Soc.* **2007**, *129*, 8801−8810.

(57) Solomon, E. I.; Szilagyi, R. K.; George, S. D.; Basumallick, L. *Chem. Rev.* **2004**, *104*, 419−458.

(58) Lewis, E. A.; Tolman, W. B. *Chem. Rev.* **2004**, *104*, 1047−1076.

(59) Farver, O.; Pecht, I. *Coord. Chem. Rev.* **2011**, *255*, 757−773.

(60) Bessho, T.; Constable, E. C.; Grätzel, M.; Redondo, A. H.; Housecroft, C. E.; Kylberg, W.; Nazeeruddin, M. K.; Neuburger, M.; Schaffner, S. *Chem. Commun.* **2008**, *32*, 3717−3719.

(61) Zhang, Q.; Zhou, Q.; Cheng, Y.; Wang, L.; Ma, D.; Jing, X.; Wang, F. *Adv. Funct. Mater.* **2006**, *16*, 1203−1208.

(62) Smith, C. S.; Branham, C. W.; Marquardt, B. J.; Mann, K. R. *J. Am. Chem. Soc.* **2010**, *132*, 14079−14085.

10552

dx.doi.org/10.1021/ja3028873 | *J. Am. Chem. Soc.* 2012, 134, 10543−10553

(63) Hsu, C.-W.; Lin, C.-C.; Chung, M.-W.; Chi, Y.; Lee, G.-H.; Chou, P.-T.; Chang, C.-H.; Chen, P.-Y. *J. Am. Chem. Soc.* **2011**, *133*, 12085−12099.

(64) Tran, D.; Ryu, C. K.; Ford, P. C. *Inorg. Chem.* **1994**, *33*, 5957−5959.

(65) Campagna, S.; Puntoriero, F.; Nastasi, F.; Bergamini, G.; Balzani, V. *Top. Curr. Chem.* **2007**, *280*, 117−214.

(66) Kume, S.; Murata, M.; Ozeki, T.; Nishihara, H. *J. Am. Chem. Soc.* **2005**, *127*, 490−491.

(67) Umeki, S.; Kume, S.; Nishihara, H. *Chem. Lett.* **2010**, *39*, 204−205.

(68) Nomoto, K.; Kume, S.; Nishihara, H. *J. Am. Chem. Soc.* **2009**, *131*, 3830−3831.

(69) Kume, S.; Nomoto, K.; Kusamoto, T.; Nishihara, H. *J. Am. Chem. Soc.* **2009**, *131*, 14198−14199.

(70) Kume, S.; Nishihara, H. *Chem. Commun.* **2011**, *47*, 415−417.

(71) Kume, S.; Nishihara, H. *Dalton Trans.* **2011**, *40*, 2299−2305.

(72) Nishikawa, M.; Nomoto, K.; Kume, S.; Inoue, K.; Sakai, M.; Fujii, M.; Nishihara, H. *J. Am. Chem. Soc.* **2010**, *132*, 9579−9581.

(73) Photoresponsive coordinated ligand rotational isomerization, such as based on a rhenium⚌carbon double bond, has been reported. McCormick, F. B.; Kiel, W. A.; Gladysz, J. A. *Organometallics* **1982**, *1*, 405−408.

(74) Schmittel, M.; Michel, C.; Wiegrefe, A.; Kalsani, V. *Synthesis* **2001**, *10*, 1561−1567.

(75) Schmittel, M.; Ganz, A. *Chem. Commun.* **1997**, 999−1000.

(76) Schmittel, M.; Michel, C.; Liu, S.-X.; Schildbach, D.; Fenske, D. *Eur. J. Inorg. Chem.* **2001**, 1155−1166.

(77) Pallenberg, A. J.; Koenig, K. S.; Barnhart, D. M. *Inorg. Chem.* **1995**, *34*, 2833−2840.

(78) Hsieh, H.-Y.; Lin, C.-H.; Tu, G.-M.; Chi, Y.; Lee, G.-H. *Inorg. Chim. Acta* **2009**, *362*, 4734−4739.

(79) Medwid, J. B.; Paul, R.; Baker, J. S.; Brockman, J. A.; Du, M. T.; Hallett, W. A.; Hanifin, J. W.; Hardy, R. A.; Tarrant, M. E.; Torley, L. W.; Wrenn, S. *J. Med. Chem.* **1990**, *33*, 1230−1241.

(80) Lafferty, J. J.; Case, F. H. *J. Org. Chem.* **1967**, *32*, 1591−1596.

(81) The sample of $1^+BF_4^-$, which contained a slight amount of CH_2Cl_2, was employed for the experiments in the manuscript, considering the elemental analysis results; the weight ratio of CH_2Cl_2 to $1^+BF_4^-$ is 1%. ^1H NMR measurement in CD_2Cl_2 revealed a presence of the residual dichloromethane (Supporting Information Figure S2), considering the reported values.[82] For clarity, we omitted the remaining solvent.

(82) Fulmer, G. R.; Miller, A. J. M.; Sherden, N. H.; Gottlieb, H. E.; Nudelman, A.; Stoltz, B. M.; Bercaw, J. E.; Goldberg, K. I. *Organometallics* **2010**, *29*, 2176−2179.

(83) Electrochemical methods for a square scheme, such as interpretation for convergence of redox waves and simulation of voltammograms, are well-established. (a) Bard, A. J.; Faulkner, L. R. *Electrochemical Methods, Fundamentals and Applications*, 2nd ed.; Wiley: New York, 2001. (b) Jacq, J. *J. Electroanal. Chem.* **1971**, *29*, 149−180. (c) Carano, M.; Echegoyen, L. *Chem.—Eur. J.* **2003**, *9*, 1974−1981. (d) Lerke, S. A.; Evans, D. H.; Feldberg, S. W. *J. Electroanal. Chem.* **1990**, *296*, 299−315.

(84) The activation energies for the i- → o-isomerization, E_a, in the copper(I) and copper(II) states, estimated from the slope of the Arrhenius plots, are 67 and 35 kJ mol^{-1}, respectively.

(85) The redox potential of cerium(IV)/(III) in water is known to be 1.36 V vs DMFc$^{+/0}$ in CH_2Cl_2, which is enough positive to oxidize the copper(I) complexes. Connelly, N. G.; Geiger, W. E. *Chem. Rev.* **1996**, *96*, 877−910.

(86) The redox potential in the excited state was estimated according to a well-established method. Juris, A.; Balzani, V.; Barigelletti, F.; Campagna, S.; Belser, P.; von Zelewsky, A. *Coord. Chem. Rev.* **1988**, *84*, 85−277.

(87) Fery-Forgues, S.; Delavaux-Nicot, B. *J. Photochem. Photobiol. A* **2000**, *132*, 137−159.

(88) It is considered that several undesired reactions can contribute to a deactivation for the i-Cu^I → o-Cu^I photorotation. For example,

the back electron transfer process, i-Cu^{II} + DMFc^0 → i-Cu^I + DMFc$^+$, can compete with the rotation in the copper(II) state, i-Cu^{II} → o-Cu^{II}. For another example, both radiative and nonradiative transition of the photoexcited state, *i-Cu^I → i-Cu^I + $h\nu'$ or heat, can compete with the PET process, *i-Cu^I + DMFc$^+$ → i-Cu^{II} + DMFc^0. Energy transfer in the photoexcited states also contributes to the deactivation. One or more of them can be the reason why the i-Cu^I → o-Cu^I photorotation is slow, considering that the sufficient light-induced voltammograms changes require long (60 min) irradiation time in the DMFc$^+$ system. However, these deactivation processes are not critical to stop the photodriven rotation.

(89) Merrill, C. L.; Wilson, L. J.; Thamann, T. J.; Loehr, T. M.; Ferris, N. S.; Woodruff, W. H. *J. Chem. Soc., Dalton Trans.* **1984**, 2207−2221.

(90) Tabbì, G.; Cassino, C.; Cavigiolio, G.; Colangelo, D.; Ghiglia, A.; Viano, I.; Osella, D. *J. Med. Chem.* **2002**, *45*, 5786−5796.

(91) Altomare, A.; Cascarano, G.; Giacovazzo, C.; Guagliardi, A.; Burla, M. C.; Polidori, G.; Camalli, M. *J. Appl. Crystallogr.* **1994**, *27*, 435.

(92) Sheldrick, G. M. *Acta Crystallogr.* **2008**, *A64*, 112−122.

(93) Farrugia, L. J. *J. Appl. Crystallogr.* **1999**, *32*, 837−838.